Bimetallic Nanophosphides

Deutsche Ausgabe: DOI: 10.1002/ange.201503386
Internationale Ausgabe: DOI: 10.1002/anie.201503386

Controlled Anisotropic Growth of Co-Fe-P from Co-Fe-O Nanoparticles**

*Adriana Mendoza-Garcia, Huiyuan Zhu, Yongsheng Yu, Qing Li, Lin Zhou, Dong Su, Matthew J. Kramer, and Shouheng Sun**

Abstract: *A facile approach to bimetallic phosphides, Co-Fe-P, by a high-temperature (300°C) reaction between Co-Fe-O nanoparticles and trioctylphosphine is presented. The growth of Co-Fe-P from the Co-Fe-O is anisotropic. As a result, Co-Fe-P nanorods (from the polyhedral Co-Fe-O nanoparticles) and sea-urchin-like Co-Fe-P (from the cubic Co-Fe-O nanoparticles) are synthesized with both the nanorod and the sea-urchin-arm dimensions controlled by Co/Fe ratios. The Co-Fe-P structure, especially the sea-urchin-like $(Co_{0.54}Fe_{0.46})_2P$, shows enhanced catalysis for the oxygen evolution reaction in KOH with its catalytic efficiency surpassing the commercial Ir catalyst. Our synthesis is simple and may be readily extended to the preparation of other multimetallic phosphides for important catalysis and energy storage applications.*

Transition-metal phosphides (M-Ps) are an important class of functional materials with interesting catalytic, magnetic, electronic, and mechanical properties.[1] In recent years, notable efforts have been devoted to the study of nanostructured M-Ps as potential noble-metal free magnets[2] for permanent magnet applications, as new catalysts for hydrogenation[3] and electrochemical reduction/oxidation reactions,[4,5] and as conductive supports to improve Li-ion battery performance.[6] Nanostructured M-Ps are often prepared by reacting a metal complex with inorganic phosphorus or an organic phosphine.[1b] They can also be produced by reacting metal oxide particles with an organic phosphine, in which the metal oxide particles are dissolved to facilitate the M-P formation.[7] Despite the synthetic controls achieved on size, composition, and structure, it has been difficult to extend these methods to prepare multimetallic phosphides (M^1M^2-Ps). A common issue in the attempted synthesis of M^1M^2-P is the uncontrolled formation of a variety of phases that are often difficult to separate, making it impossible to study synergistic effects of different metals on physical and chemical properties of the M^1M^2-Ps.

Recently, we became interested in studying the multimetallic effect on magnetic and catalytic properties of nanostructured phosphides. We tested the synthesis of Co-Fe-Ps in a high-temperature organic phase reaction with pre-made Co-Fe-O NPs as precursors, aiming to achieve the desired phase, dimension, and composition controls. We found that after mixing metal oxide Co-Fe-O nanoparticles (NPs) with trioctylphosphine (TOP) and allowing them to react at 300°C, O was exchanged by P, leading to total phosphidation of these Co-Fe-O NPs into Co-Fe-P. The Co/Fe ratio in the final Co-Fe-P product was controlled by the amount of Co and Fe in the precursor NPs. More interestingly, we noticed that the phosphide growth direction was anisotropic and one-dimensional nanostructures were formed. The final shapes of the Co-Fe-Ps were controlled by the initial morphology of the oxide NPs. The polyhedral oxide NPs yielded Co-Fe-P nanorods while the cubic NPs led to the formation of sea-urchin-like Co-Fe-P. These phosphides, and particularly the sea-urchin-like $(Co_{0.54}Fe_{0.46})_2P$, exhibited interesting catalytic properties towards the oxygen evolution reaction in 0.1M KOH, with higher activity than Co_2P, Fe_2P, and even the commercial Ir catalyst.

The Co-Fe-O NPs were cobalt ferrite ($CoFe_2O_4$)-based and the Co/Fe ratios were controlled so that Co-Fe-O could have different Co/Fe compositions from Co-rich to Fe-rich, denoted as $Co_xFe_{3-x}O_4$ ($0 < x \leq 2$). Composition-independent 25–30 nm oxide NPs were synthesized by thermal decomposition of $[Fe(acac)_3]$ and $[Co(acac)_2]$ (acac = acetylacetonate) in benzyl ether[8] (Supporting Information). Polyhedral NPs were formed when oleylamine and oleic acid were used as surfactants. Adding sodium oleate into the reaction solution led to the formation of cubic NPs. In both cases, the x in $Co_xFe_{3-x}O_4$ was controlled by the molar ratio of $[Co(acac)_2]/[Fe(acac)_3]$. Figure 1A shows a typical transmission electron microscopy (TEM) image of about 25 nm $Co_{1.14}Fe_{1.86}O_4$ polyhedral NPs. Elemental mappings taken by energy-filtered TEM (EFTEM) show the uniform distribution of Fe, Co, and O across each NP (Figure 1B–D). Similar

[*] A. Mendoza-Garcia, Dr. H. Zhu,[+] Prof. Y. Yu,[++] Dr. Q. Li, Prof. S. Sun
Department of Chemistry, Brown University
Providence, RI 02912 (USA)
E-mail: ssun@brown.edu
Dr. L. Zhou, Prof. M. J. Kramer
The Ames Laboratory, US Department of Energy
Iowa State University, Ames, IA 50011 (USA)
Dr. D. Su
Center for Functional Nanomaterials
Brookhaven National Laboratory, Upton, NY 11973 (USA)
[+] Present address: Chemical Sciences Division
Oak Ridge National Laboratory, Oak Ridge, TN 37831 (USA)
[++] Present address: School of Chemical Engineering and Technology
Harbin Institute of Technology
Harbin, Heilongjiang 150001 (China)

[**] This work was supported by the U.S. Department of Energy, Office of Energy Efficiency and Renewable Energy (EERE), under its Vehicle Technologies Program, through the Ames Laboratory. The Ames Laboratory is operated by Iowa State University under contract DE-AC02-07CH11358. Electron microscopy work carried out at the Center for Functional Nanomaterials, Brookhaven National Laboratory was supported by the U.S. Department of Energy, Office of Basic Energy Sciences under Contract No. DE-AC02-98CH10886.
Supporting information for this article is available on the WWW under http://dx.doi.org/10.1002/anie.201503386.

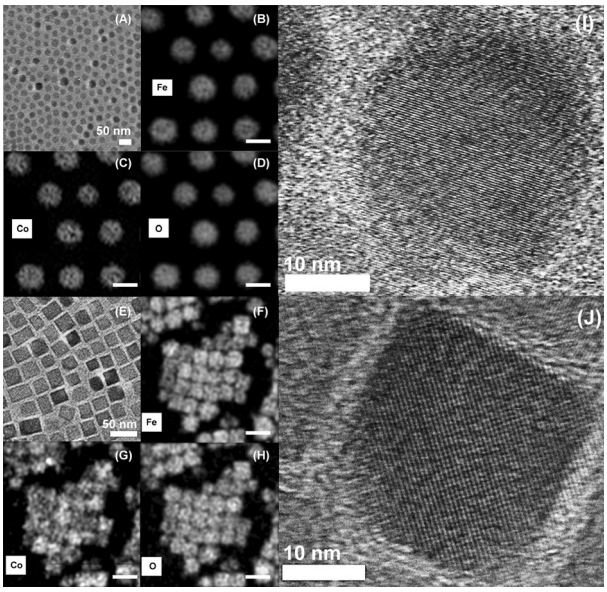

Figure 1. A) TEM image of the as-synthesized polyhedral $Co_{1.14}Fe_{1.86}O_4$ NPs and B)–D) their E FTEM elemental mappings, illustrating the distribution of B) Fe, C) Co, and D) O across the NPs. E) TEM image of the as-synthesized cubic $Co_{1.32}Fe_{1.68}O_4$ NPs and F)–H) their corresponding EFTEM elemental mappings, showing the distribution of F) Fe, G) Co, and H) O across the cubes. I), J) HRTEM images of a single polyhedral $Co_{1.14}Fe_{1.86}O_4$ NP (I) and cubic $Co_{1.32}Fe_{1.68}O_4$ NP (J). Scale bars on EFTEM images correspond to 50 nm.

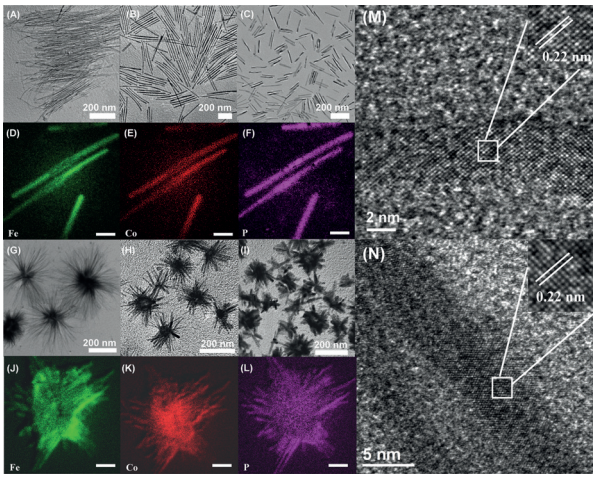

Figure 2. A)–C) TEM images of the Co-Fe-P nanorods, showing the composition dependence of the length and thickness: A) $(Co_{0.16}Fe_{0.84})_2P$, B) $(Co_{0.47}Fe_{0.53})_2P$, and C) $(Co_{0.79}Fe_{0.21})_2P$. D)–F) EFTEM elemental mappings of $(Co_{0.47}Fe_{0.53})_2P$, illustrating the distribution of D) Fe, E) Co, and F) P in the structure. G)–I) TEM images of the sea-urchin-like Co-Fe-P, showing the composition-dependent dimension change of the nanourchin arms: G) $(Co_{0.24}Fe_{0.76})_2P$, H) $(Co_{0.54}Fe_{0.46})_2P$, and I) $(Co_{0.75}Fe_{0.25})_2P$. J)–L) EFTEM elemental mappings showing distribution of Fe, Co, and P across a representative $(Co_{0.54}Fe_{0.46})_2P$ sea-urchin structure. M), N) HRTEM images of the section of a $(Co_{0.47}Fe_{0.53})_2P$ nanorod (M) and the arm of one $(Co_{0.54}Fe_{0.46})_2P$ nanourchin (N), with their respective insets showing a zoom-in of a representative local area. Scale bars shown in all of the EFTEM images correspond to 25 nm.

characterizations were also performed on circa 30 nm cubic $Co_{1.32}Fe_{1.68}O_4$ NPs (Figure 1 F–I). The cubes are uniform in size and shape with Fe, Co, and O homogeneously distributed. High-resolution TEM (HRTEM) images of a polyhedral NP (Figure 1 I) and a cube (Figure 1 J) further confirm the formation of single crystalline structures, both having lattice fringe spacings of 0.29 nm, which corresponds to the interplanar spacing of (220) planes from the inverse spinel variant of ferrite.

To convert Co-Fe-O into Co-Fe-P, 20 mg of Co-Fe-O NPs were dispersed in a mixture of 10 mL of 1-octadecene, 2 mL of oleylamine, and 4 mL of TOP (10 mmol), and the dispersion was heated at 300 °C for 12 h to allow a complete phosphidation process (Supporting Information). As phosphidation occurs, the polyhedral NPs grow into nanorods. The composition, as well as the length and thickness of these nanorods were determined by the molar ratio of Co/Fe from the oxide NPs. For example, reacting $Co_{0.24}Fe_{2.76}O_4$ NPs with TOP produced $(Co_{0.16}Fe_{0.84})_2P$ nanorods with length of circa 450 nm and an average diameter of 5 nm (denoted as 450 nm × 5 nm nanorods, Figure 2 A). When the starting oxide NPs were $Co_{1.14}Fe_{1.86}O_4$ or $Co_{1.99}Fe_{1.01}O_4$ NPs, 330 nm × 10 nm $(Co_{0.47}Fe_{0.53})_2P$ nanorods (Figure 2 B), or 150 nm × 14 nm $(Co_{0.79}Fe_{0.41})_2P$ nanorods (Figure 2 C) were obtained. The distribution of the elements on the $(Co_{0.47}Fe_{0.53})_2P$ nanorods was studied by EFTEM (Figure 2 D–F). The uniform Fe, Co, P mappings shown across individual rods indicate that all three elements are uniformly distributed along the rod, confirming the formation of a solid solution structure in Co-Fe-P. However, if the x value exceeds 0.79 in $(Co_xFe_{1-x})_2P$, the nanorods could not be formed; instead, the phosphide adopted a morphology similar to that of hollow spherical Co_2P NPs (Supporting Information, Figure S1 A).

After reacting Co-Fe-O nanocubes with TOP, sea-urchin-like Co-Fe-P were formed. The urchin-arm dimensions were controlled by the amount of Fe, which is similar to the case when the polyhedral Co-Fe-O NPs were used to grow Co-Fe-P; the more Fe in the structure, the longer and thinner the arms. For example, reacting $Co_{0.42}Fe_{2.58}O_4$ with TOP yielded sea-urchin-like $(Co_{0.24}Fe_{0.76})_2P$ with the average dimension of each arm being 200 nm × 2 nm, denoted as 200 × 2 nm nanourchins (Figure 2 G). Phosphidation of $Co_{1.32}Fe_{1.68}O_4$ gave 80 nm × 5 nm $(Co_{0.54}Fe_{0.46})_2P$ nanourchins (Figure 2 H), and of $Co_{1.98}Fe_{1.02}O_4$ produced 60 nm × 10 nm $(Co_{0.75}Fe_{0.25})_2P$ nanourchins (Figure 2 I). The center of the sea urchins appears to be hollow (Supporting Information, Figure S2), indicating that during the P/O exchange process the O outward diffusion is faster than the P inward diffusion, similar to what is described in a typical nanoscale Kirkendall effect.[9] To verify the formation of a single phosphide phase, the distribution of the elements within a representative $(Co_{0.54}Fe_{0.46})_2P$ sea urchin was studied by EFTEM (Figure 2 K–L). The elemental mappings imply again the formation of a homogeneous solid solution in the Co-Fe-P structure. The uniformity of the nanorods and the sea urchin arms was also characterized by HRTEM. Figure 2 M shows the HRTEM of a section of a $(Co_{0.47}Fe_{0.53})_2P$ nanorod, and Figure 2 N shows a representative arm of a $(Co_{0.54}Fe_{0.46})_2P$ nanourchin. In both structures,

the lattice fringe distance was about 0.22 nm, which is close to the interplanar spacing of (111) planes in the hexagonal Fe_2P and of (121) planes in orthorhombic Co_2P. We should note that the sea-urchin formation is *x*-dependent. If *x* in the $(Co_xFe_{1-x})_2P$ composition falls outside of the range of $0.24 \leq x \leq 0.75$, the Co-rich product adopts Co_2P-like hollow spherical shape while the Fe-rich phosphide has the Fe_2P-like nanowire structure (Supporting Information, Figure S1 A–B).

To understand the Co-Fe-O shape-dependent growth of Co-Fe-P, the growth process was monitored by collecting samples at different reaction times for TEM analyses, as summarized in the Supporting Information, Figure S3. When polyhedral NPs react with TOP (Supporting Information, Figure S3 A–E), some rods are formed after only 1.5 h of reaction. Also, in some NPs, it is possible to see how "rod-like" protuberances emerge from their surface, indicating the growth of M-P from the M-O surface. Images after 3, 6, and 12 h of reaction show the progressive formation/elongation of the rods as a consequence of the phosphidation of all of the oxide NPs. The exposed planes on these single-crystal structures (generally (311) or (111))[8] are readily available for P diffusion, and therefore growth along a single direction is observed. On the other hand, when the nanocubes are used as seeds (Supporting Information, Figure S3 F–J), it can be seen that after 1.5 h of reaction the cubes initially adopt concave shapes that later grow into the sea-urchin structures. It is known that oleate binds slightly more strongly to (100) planes on metal oxide surfaces.[10] During the early stage of phosphidation, the oleate hinders the P diffusion on the (100) planes, favoring the M-P growth along $<111>/<110>$ directions into the concave shape and further into the sea-urchin structure. The nanourchin structure formation is due to the associated growth of the circularly distorted Co_2P and the wire shaped Fe_2P[11] (Supporting Information, Figure S1).

The complete transformation of the Co-Fe-O nanocubes into Co-Fe-P nanourchins was confirmed by X-ray diffraction (XRD) patterns (Figure 3 A). The patterns show the change from a face-centered cubic ferrite structure into a Fe_2P-Co_2P solid solution structure.[12] Similar results were found when polyhedral oxide NPs were converted into phosphide nanorods (Supporting Information, Figure S4). The structural transformation was further verified by the change of magnetic properties of the samples (Figure 3 B). The as-synthesized $Co_{1.32}Fe_{1.68}O_4$ nanocubes show a room temperature coercivity of 545 Oe and a saturation magnetization of 35 emu g^{-1}. These values are considerably reduced after a full conversion into $(Co_{0.54}Fe_{0.46})_2P$ that have no coercivity and very low magnetization of 0.35 emu g^{-1}, which is consistent with the weak magnetic behavior observed from $(Co\text{-}Fe)_2P$.[12] Similar results were also observed when polyhedral oxide NPs were converted into the phosphides (Supporting Information, Figure S4).

M-Ps have regained great attention as earth-abundant active catalysts for water splitting.[13] Theoretical studies predict that the synergistic interaction between Co and Fe can help to weak the adsorption energies of some catalytic species, decreasing the overpotential of the oxygen evolution reaction (OER) in alkaline media.[14] Our Co-Fe-P can serve as an ideal model for the study of Co-Fe effect on OER. Here

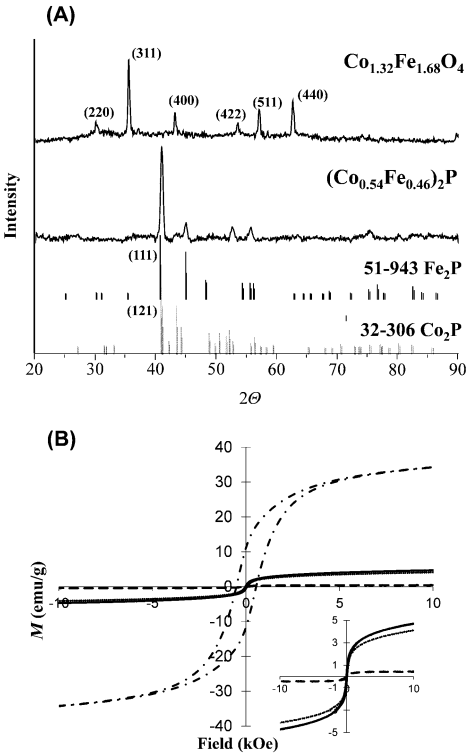

Figure 3. A) XRD patterns of the as-synthesized $Co_{1.32}Fe_{1.68}O_4$ nanocubes, $(Co_{0.54}Fe_{0.46})_2P$ sea urchins, and standard Fe_2P (JCPDS 51-943) and Co_2P (JCPDS 32-306). B) Room-temperature magnetic hysteresis loops showing the transition from the $Co_{1.32}Fe_{1.68}O_4$ nanocubes to $(Co_{0.54}Fe_{0.46})_2P$ sea urchins: As-synthesized nanocubes (–•–•), after 3 h of reaction (——), after 6 h of reaction (•••••), and after 12 h of reaction (-----). Inset: Hysteresis loops of the samples collected after 3, 6, and 12 h of reaction.

we selected the Co-Fe-P nanourchins for the initial tests. The catalyst was loaded on Ketjen carbon (C) and further on a glassy carbon rotating-disk electrode (Supporting Information). Its OER catalysis was evaluated in N_2-saturated 0.1 M KOH solution. The Co-Fe-O, Co_2P, and Fe_2P catalysts were also prepared and studied similarly. Figure 4 A summarizes the polarization curves of these catalysts as well as the commercial Ir catalyst. CoO and Fe_3O_4 are even less active than the Co_2P and Fe_2P (Supporting Information, Figure S5). We can see the $(Co_{0.54}Fe_{0.46})_2P$ requires the lowest oxidation potential to generate the same level of the OER current.

The performance of an OER catalyst is commonly measured by the overpotential required to achieve a 10 mA cm^{-2} current density per geometric area at ambient temperature and standard pressure.[15] By varying the volume of the $(Co_{0.54}Fe_{0.46})_2P$ dispersion deposited on the electrode, we obtained the lowest potential, 1.60 V (equal to an overpotential of 0.37 V at 10 mA cm^{-2}) when the NP amount equals 20 μg (measured by inductively coupled plasma atomic emission spectroscopy, ICP-AES; Supporting Information, Figure S6). This overpotential value is also lower than those obtained from $Co_{1.32}Fe_{1.68}O_4$ and commercial Ir (Figure 4 B). Given the enhanced activity of the Co-Fe-P system with respect to Co-Fe-O and Ir, we conclude that the metal phosphide structure helps to improve the electronic conduc-

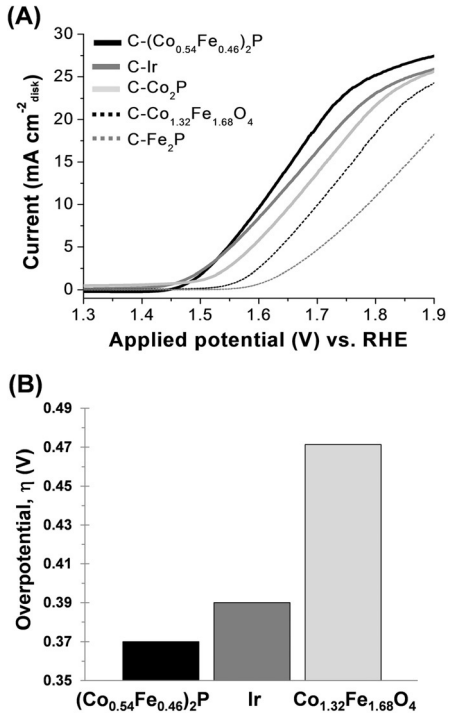

Figure 4. A) OER polarization curves of the $(Co_{0.54}Fe_{0.46})_2P$, commercial Ir, Co_2P, $Co_{1.32}Fe_{1.68}O_4$, and Fe_2P catalysts. B) Overpotentials of the $(Co_{0.54}Fe_{0.46})_2P$, $Co_{0.4}Fe_{2.6}O_4$, and commercial Ir catalysts for the OER at 10 mA cm^{-2}. For all of the tests, the catalyst amount on the glassy carbon electrode was 20 μg of NPs (equivalent to 200 μg (NPs + C) cm^{-2} loading) and the catalysts were evaluated in N_2-saturated 0.1 M KOH at a scan rate of 10 mV s^{-1} at 1600 rpm.

tivity of the catalyst. The OER catalysis of the $(Co_{0.54}Fe_{0.46})_2P$ could be further increased if the OER was studied in an alkaline solution with higher KOH concentration (Supporting Information, Figure S7). For example, in 1.0 M KOH, the oxidation potential at 10 mA cm^{-2} is lowered to 1.51 V, which is equal to an overpotential of 0.28 V (0.29 V for the commercial Ir). These observations support the previous prediction that Co and Fe in the Co-Fe-P structure do show a synergistic interaction that enhances the OER catalysis.

In summary, this work presents a facile approach to nanostructured bimetallic phosphides via high-temperature (300 °C) reaction of metal oxide NPs with TOP. In the synthesis, the co-presence of Co and Fe in the Co-Fe-O NPs facilitates the anisotropic growth of Co-Fe-P into either nanorods (when the Co-Fe-O NPs are in polyhedral shape) or sea urchins (when the Co-Fe-O NPs are in cubic shape). The dimensions of the nanorods and the arms of the nanourchins are controlled by Co/Fe ratios. The Co-Fe-P NPs show enhanced catalysis for OER and the catalytic efficiency of the $(Co_{0.54}Fe_{0.46})_2P$ nanourchin even surpasses the Ir-catalyst. Our synthesis is simple and general to prepare uniform M^1M^2-Ps. It can be potentially extended to the preparation of other M-Ps and metal phosphates as well, providing a new approach to metal phosphides and phosphates with control of nanoscale structure and dimension for important catalysis and energy storage applications.

Keywords: cobalt–iron phosphides · metal oxide phosphidation · nanorods · oxygen evolution reaction

How to cite: *Angew. Chem. Int. Ed.* **2015**, *54*, 9642–9645
Angew. Chem. **2015**, *127*, 9778–9781

[1] a) S. L. Brock, K. Senevirathne, *J. Solid State Chem.* **2008**, *181*, 1552–1559; b) R. Prins, M. E. Bussell, *Catal. Lett.* **2012**, *142*, 1413–1436.
[2] F. Luo, H.-L. Su, W. Song, Z.-M. Wang, Z.-G. Yan, C.-H. Yan, *J. Mater. Chem.* **2004**, *14*, 111–115.
[3] S. T. Oyama, T. Gott, H. Y. Zhao, Y. K. Lee, *Catal. Today* **2009**, *143*, 94–107.
[4] a) E. J. Popczun, J. R. McKone, C. G. Read, A. J. Biacchi, A. M. Wiltrout, N. S. Lewis, R. E. Schaak, *J. Am. Chem. Soc.* **2013**, *135*, 9267–9270; b) E. J. Popczun, C. G. Read, C. W. Roske, N. S. Lewis, R. E. Schaak, *Angew. Chem. Int. Ed.* **2014**, *53*, 5427–5430; *Angew. Chem.* **2014**, *126*, 5531–5534.
[5] J. Kupka, A. Budniok, *J. Appl. Electrochem.* **1990**, *20*, 1015–1020.
[6] a) P. S. Herle, B. Ellis, N. Coombs, L. F. Nazar, *Nat. Mater.* **2004**, *3*, 147–152; b) W. Ojczyk, J. Marzec, K. Swierczek, W. Zajac, M. Molenda, R. Dziembaj, J. Molenda, *J. Power Sources* **2007**, *173*, 700–706.
[7] E. Muthuswamy, S. L. Brock, *J. Am. Chem. Soc.* **2010**, *132*, 15849–15851.
[8] Y. Yu, A. Mendoza-Garcia, B. Ning, S. Sun, *Adv. Mater.* **2013**, *25*, 3090–3094.
[9] W. Wang, M. Dahl, Y. Yin, *Chem. Mater.* **2013**, *25*, 1179–1189.
[10] L. H. Wu, P. O. Jubert, D. Berman, W. Imaino, A. Nelson, H. Y. Zhu, S. Zhang, S. H. Sun, *Nano Lett.* **2014**, *14*, 3395–3399.
[11] a) A. T. Kelly, I. Rusakova, T. Ould-Ely, C. Hofmann, A. Lüttge, K. H. Whitmire, *Nano Lett.* **2007**, *7*, 2920–2925; b) D.-H. Ha, L. M. Moreau, C. R. Bealing, H. Zhang, R. G. Hennig, R. D. Robinson, *J. Mater. Chem.* **2011**, *21*, 11498–11510.
[12] a) K. J. De Vos, W. a. J. J. Velge, M. G. V. D. Steeg, H. Zijlstra, *J. Appl. Phys.* **1962**, *33*, 1320–1322; b) W. Q. Huang, G. F. Huang, B. Liang, C. L. Xie, *J. Magn. Magn. Mater.* **2009**, *321*, 1177–1181.
[13] P. W. Du, R. Eisenberg, *Energy Environ. Sci.* **2012**, *5*, 6012–6021.
[14] M. Bajdich, M. Garcia-Mota, A. Vojvodic, J. K. Norskov, A. T. Bell, *J. Am. Chem. Soc.* **2013**, *135*, 13521–13530.
[15] C. C. L. McCrory, S. H. Jung, J. C. Peters, T. F. Jaramillo, *J. Am. Chem. Soc.* **2013**, *135*, 16977–16987.

Received: April 14, 2015
Revised: May 15, 2015
Published online: June 26, 2015

